Protein–Tyrosyl Radical Interactions in Photosystem II Studied by Electron Spin Resonance and Electron Nuclear Double Resonance Spectroscopy: Comparison with Ribonucleotide Reductase and in Vitro Tyrosine†

Curtis W. Hoganson and Gerald T. Babcock*

Department of Chemistry, Michigan State University, East Lansing, Michigan 48824-1322

Received June 10, 1992; Revised Manuscript Received September 23, 1992

ABSTRACT: The stable tyrosine radical in photosystem II, $Y_D^{\bullet}$, has been studied by ESR and ENDOR spectroscopies to obtain proton hyperfine coupling constants from which the electron spin density distribution can be deduced. Simulations of six previously published ESR spectra of PSII (one at Q band; five at X band, of which two were after specific deuteration and two others were of oriented membranes) can be achieved by using a single set of magnetic parameters that includes anisotropic proton hyperfine tensors, an anisotropic **g** tensor, and noncoincident axis systems for the **g** and **A** tensors. From the spectral simulation of the oriented samples, the orientation of the phenol head group of $Y_D^{\bullet}$ with respect to the membrane plane has been determined. A similar orientation for $Y_Z^{\bullet}$, the redox-active tyrosine in PSII that mediates electron transfer between P680 and the oxygen-evolving complex, is expected. ENDOR spectra of $Y_D^{\bullet}$ in PSII preparations from spinach and *Synechocystis* support the set of hyperfine coupling constants but indicate that small differences between the two species exist. Comparison with the results of spectral simulations for tyrosyl radicals in ribonucleotide reductase from prokaryotes or eukaryotes and with in vitro radicals indicates that the spin density distribution remains that of an odd-alternant radical but that interactions with the protein can shift spin density within this basic pattern. The largest changes in spin density occur at the tyrosine phenol oxygen and at the ring carbon para to the oxygen, which indicates that mechanisms exist in the protein environment for fine-tuning the chemical and redox properties of the radical species.

Amino acid radicals are now known as essential participants in the reactions of a growing number of enzymes [for a review, see Stubbe (1989)]. Their utility for catalysis apparently derives from their thermodynamic instability: they tend to oxidize or to abstract hydrogen atoms from other molecules. Yet in enzymes, they can be stable as radicals, even for as long as a week at 4 °C, as is the case for the tyrosyl radical in purified ribonucleotide reductase. Clearly, the protein environment surrounding a free radical can stabilize it in some way and prevent nonphysiological reactions.

Tyrosine radicals are the natural systems for investigating these questions, because the oxidized, paramagnetic form of this amino acid is essential for function in RDPR[1] (Sjöberg & Gräslund, 1983), photosystem II (Barry & Babcock, 1987), and prostaglandin H synthase (Smith et al., 1992), and tyrosine-derived radicals are found in galactose oxidase (Whittaker & Whittaker, 1990) and in amine oxidases (Jones et al., 1990). Of the 20 common amino acid constituents of proteins, tyrosine, having an E_0' in neutral, aqueous solution of +0.93 V vs NHE (DeFelippis et al., 1989, 1991), is among the most easily oxidized. The relative ease by which the tyrosine phenol group can be oxidized and the potential for modulation of the chemical and redox properties of the resulting radical most likely account for its widespread occurrence as a catalytically important paramagnetic species. The cysteine side chain, which is oxidized to its thiyl form in a one-electron process, has a redox potential similar to that of tyrosine in neutral solutions (Prütz et al., 1986) but is rapidly oxidized further by O_2 (Sevilla et al., 1989). Radicals of tryptophan, the next most easily oxidized amino acid, with E_0' of +1.05 V (DeFelippis et al., 1989, 1991), are important for function in cytochrome *c* peroxidase (Scholes et al., 1989; Sivaraja et al., 1989) and in *Escherichia coli* photolyase (Li et al., 1991). In an interesting recent development, the free radical in pyruvate formate-lyase has been shown to originate from a glycine species (Wagner et al., 1992).

The realization that redox-active amino acids are widely used in enzyme catalysis has been made only recently and an understanding as to how the protein environment controls these unstable and highly reactive species has not yet emerged. The obvious analytical tool for addressing these issues is electron spin resonance spectroscopy, which specifically detects paramagnetic entities. In combination with ENDOR spectroscopy and spectral simulation, ESR can be used to determine hyperfine coupling constants to protons of the radical in model and protein systems. From these coupling constants, the amount of unpaired spin at adjacent carbon atoms can be determined. A detailed analysis of ENDOR spectra from RDPR of *E. coli*, for example, gave a complete determination of the spin densities at the seven atoms of the tyrosine phenoxyl radical (Bender et al., 1989); this distribution followed an odd-alternant pattern with substantial spin density at the phenol oxygen and at the ring positions ortho and para to the oxygen substituent. Recent data on the cysteine-substituted tyrosyl radical in galactose oxidase (Babcock et al., 1992) show that in this system, as well, the basic odd-alternant pattern is preserved, despite the perturbation introduced by the ortho thioether substituent. From the RDPR work, the values of the proportionality constants between unpaired electron spin densities and hyperfine coupling constants for various classes of protons were determined (Bender et al., 1989). These can

† This work was supported by the USDA Competitive Grants Office and NIH Grant GM37300.

[1] Abbreviations: ENDOR, electron nuclear double resonance; ESR, electron spin resonance (or equivalently, electron paramagnetic resonance, EPR); PSII, photosystem II; RDPR, ribonucleoside diphosphate reductase; $Y_D^{\bullet}$, the stable tyrosine radical of PSII; $Y_Z^{\bullet}$, the tyrosine radical in PSII that transfers electrons between the reaction center chlorophyll, P680, and the manganese ensemble in the oxygen-evolving complex.

0006-2960/92/0431-11874$03.00/0

be used in McConnell relations to calculate spin densities from the hyperfine coupling constants of other tyrosyl radicals.

We focus on the stable tyrosine radical of PSII, $Y_D^{\bullet}$, in the present work. Although not absolutely essential for growth or PSII function (Debus et al., 1988), all wild-type, oxygen-evolving photosynthetic organisms possess this radical. Furthermore, the redox-active tyrosyl residue of PSII essential for O_2 evolution, $Y_Z^{\bullet}$, has an ESR spectrum nearly identical to that of the stable radical [for reviews, see Babcock et al. (1989) and Rutherford et al. (1992)]. In this work, we have analyzed previously published ESR spectra of this radical to arrive at a set of proton hyperfine coupling constants that can account for all the published spectra. We present ENDOR spectra to support these assignments and show that the data can be used to determine the orientation of the tyrosine radical in the PSII membrane. Finally, we compare our results for $Y_D^{\bullet}$ with those obtained by simulating analogous ESR data for ribonucleotide reductase and model tyrosine radicals. We conclude that spin density distributions in tyrosine radicals within proteins retain the basic odd-alternant pattern (Barry et al., 1990) but that, within this framework, substantial differences between the various protein bound radicals can occur, presumably by interactions with neighboring amino acids.

MATERIALS AND METHODS

Reaction center complexes from spinach were prepared as described by Ghanotakis et al. (1987) and resuspended in 0.4 M sucrose, 20 mM NaCl, and 50 mM MES (pH 6.5). *Synechocystis* was grown on labeled tyrosine as described previously (Barry et al., 1990). Photosystem II from *Synechocystis* was isolated as described by Noren et al. (1991) and resuspended in 25% (v/v) glycerol, 0.05% (w/v) lauryl maltoside, 20 mM $CaCl_2$, 15 mM NaCl, and 50 mM MES (pH 6.5). Samples for ENDOR were prepared by adding an equal volume of 30% (w/v) poly(ethylene glycol) (mol wt 8000) to the PSII suspension and centrifuging the resulting suspension in the quartz EPR tube.

ENDOR spectroscopy was performed at X-band with a Bruker ER200D ESR spectrometer equipped with an ER250 ENDOR accessory and an ER250ENB cavity. The magnetic field was measured with a Bruker ER035M NMR gaussmeter; the microwave frequency was measured with a HP 5245 counter/5255 3–12-GHz frequency converter. The samples were maintained at 110–140 K by cooled, flowing N_2 gas. The RF coils were described by Bender et al. (1989). In order to improve the signal-to-noise ratio, we employed simultaneous modulation of both the RF frequency and the magnetic field at 12.5 kHz and 39 Hz, respectively, with phase-sensitive detection at both frequencies, as described by Leniart (1979). The signal from the ESR bridge is phase-sensitive detected by the Bruker receiver (12.5 kHz) with a 1-ms output time constant, and the resulting signal is phase-sensitive detected by a PAR Model 126 lock-in amplifier (39 Hz). This scheme avoids the need to subtract off-resonance baseline scans, which, because of low signal amplitudes and coil-dependent baseline drifts, would otherwise be necessary.

Simulations of powder and partially oriented ESR spectra were performed by using a program (Brok et al., 1986) updated to run on personal computers and modified to include the allowed transitions of the electron coupled to spin $I = 1$ nuclei.

RESULTS

(1) Ribonucleotide Reductase. The detailed ENDOR study of *E. coli* RDPR by Bender et al. (1989) is an excellent starting point for understanding the electronic structure of tyrosyl radicals. It provides the complete set of hyperfine coupling constants necessary to interpret the ESR spectrum; and, using these values, we can simulate the ESR spectra of the tyrosyl radical in that enzyme. Although the **g**-tensor principal components are not known exactly, the isotropic value is 2.0047–2.0049 (Sahlin et al., 1982) and the anisotropy has been estimated to be 0.005–0.007 (Ehrenberg & Reichard, 1972). Thus, the **g** tensor of RDPR is similar to the **g** tensors determined for irradiated, crystalline tyrosine hydrochloride (2.0067, 2.0045, 2.0023) (Fasanella & Gordy, 1969) and for $Y_D^{\bullet}$ in PSII (2.0074, 2.0044, 2.0023) (Brok et al., 1985; Gulin et al., 1992). A good simulation of the RDPR spectrum was obtained (Figure 1) with the experimentally determined hyperfine coupling constants (Bender et al., 1989) and a **g** tensor of 2.0077, 2.0054, 2.0023, where the largest value corresponds to the C–O bond direction and the smallest value corresponds to the direction normal to the ring plane (Table I). This orientation of the **g** tensor is the same as that reported for the radical in a single crystal of tyrosine hydrochloride (Fasanella & Gordy, 1969).

As has been discussed earlier, the radical formed by one-electron oxidation of tyrosine is an odd-alternant radical with the spin localized mainly at the C1, C3, C5, and O atoms. (In

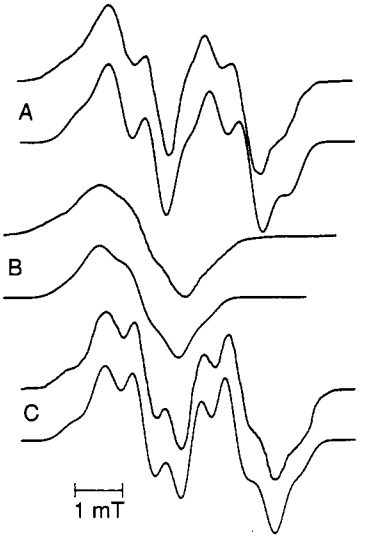

FIGURE 1: X-band ESR spectra of ribonucleotide reductase and corresponding simulation immediately below each experimental spectrum: (A) fully protonated from *E. coli*, (B) methylene-deuterated from *E. coli*, and (C) fully protonated from mouse. Experimental traces A and B are from Gräslund et al. (1985); trace C is from Sahlin et al. (1987). The parameters used in the simulations are given in Table I. One millitesla = 10 G.

Table I: Hyperfine and **g** Tensors Used in Simulations

	E. coli RDPR	mouse RDPR	PSII $Y_D^{\bullet}$	Tyr- model
g_x	2.0077	2.0074	2.0074	2.0068
g_y	2.0054	2.0044	2.0044	2.0045
g_z	2.0023	2.0023	2.0023	2.0023
$A_{3,5x}$[a]	−9.6	−9.0	−10.5	−9.75
$A_{3,5y}$	−2.8	−2.5	−3.2	−2.8
$A_{3,5z}$	−7	−6.8	−7.0	−6.8
$\Phi_{3,5}$[b]	±27	±25	±22	±22
$A_{\beta 1\parallel}$	21.2	20.8	8.3	13.0
$A_{\beta 1\perp}$	19.6	18.8	7.7	11.3
$A_{\beta 2\parallel}$	+1.75	+5.1	<2.5	<2.2
$A_{\beta 2\perp}$	−0.7	+4.8	<2.5	<2.2

[a] Hyperfine couplings given in gauss. [b] Angles $\Phi_{3,5}$ are the angles between g_x and A_x (or between g_y and A_y), given in degrees. Simulations also used a Gaussian line-width parameter and hyperfine couplings to the 2,6 protons of +1.7, +2.7, and +0.4 gauss with $\Phi_{2,6}$ of ±10°.

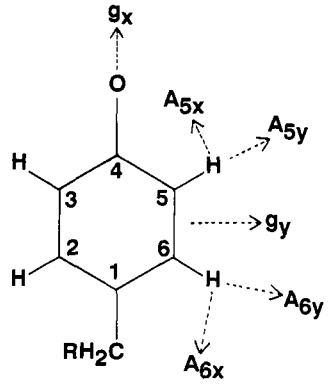

FIGURE 2: Structure of the tyrosyl radical with the numbering scheme used in this paper and the approximate directions of the principal axes of the **g** tensor and the α proton hyperfine tensors.

the numbering scheme used in this paper, the methylene group is bonded to ring carbon 1 and the oxygen is bonded to ring carbon 4; see Figure 2). The ESR line shape is determined mainly by hyperfine coupling to one proton at the methylene position and to two protons at the 3 and 5 ring positions. For an aromatic radical in which the spin density is distributed over several nuclei, the net dipolar hyperfine interaction, its principal components, and its axis system are determined by the spatial distribution of the spin density (O'Malley & Babcock, 1986). Our simulations indicate that the principal axes of the anisotropic hyperfine coupling constants of the 3 and 5 protons are aligned with the smallest value approximately along the C–H bond.

If either the methylene protons or the 3,5 protons are replaced with deuterons, the ESR spectrum becomes less complex. Good simulations were obtained after adjusting the proton hyperfine tensors by a factor of 0.154 to account for the smaller gyromagnetic ratio of the deuterium nucleus (Kurreck et al., 1988). In Figure 1, trace B, the methylene-deuterated ESR spectrum and simulation are shown. The experimental spectrum is from Gräslund et al. (1985); the spectrum shown in Bender et al. (1989) appears to be from a sample that contains a significant amount of undeuterated radical. The good agreement between experimental spectra and the simulations in Figure 1 indicate that the calculations performed by the simulation program are adequate to reproduce powder spectra of organic radicals with anisotropic hyperfine couplings and **g** tensor. Conversely, it also shows that, once the hyperfine coupling constants have been constrained by the higher resolution data available from ENDOR measurements, simulation can reproduce the experimental spectra with a minimal number of free parameters.

The spectrum of RDPR derived from eukaryotes and certain viruses differs significantly from that of RDPR from *E. coli* (Sjöberg & Gräslund, 1983; Harder & Follmann, 1987). This spectrum can be simulated (Figure 1C) by using a set of hyperfine values (Table I) similar to that described above. The major difference is the much larger coupling to the second methylene proton. A rotation of the methylene group with respect to the ring can account for this change and was suggested by Sahlin et al. (1982). Relative to *E. coli* RDPR, the two methylene protons in eukaryotic RDPR are both rotated away from the plane of the ring. For each β proton of the methylene group

$$A_{iso} \approx B_1 \rho_{C1} \cos^2 \theta_H \qquad (1)$$

where ρ_{C1} is the spin density at C1 and θ_H is the dihedral angle defined by the locations of the methylene proton, methylene carbon atom, ring carbon atom C1, and its p_z axis. The constant B_1 was determined by Fessenden and Schuler (1963) to be 58 G (162 MHz). Assuming the proton dihedral orientations to differ by 120° and using the isotropic hyperfine couplings for the two methylene protons of 19.2 and 5 G, we calculate for eukaryotic RDPR both ρ_{C1} and the two θ_H values. The results are given in Table II. We find $\theta_{H1} = 0°$ and $\rho_{C1} = 0.33$ in the mouse enzyme, whereas in *E. coli* RDPR, $\theta_{H1} = 33°$ and $\rho_{C1} = 0.49$ (Bender et al., 1989), so there appears to be a substantial difference in spin density at C1. The 3,5 proton hyperfine couplings are about 7% less than in the *E. coli* enzyme, implying only a small change in spin density at those positions. Thus, the spin density lost from C1 probably appears at the phenol oxygen, where it has only a small effect on the hyperfine splittings but causes a slight rotation of the 3,5 hyperfine tensors relative to the *E. coli* enzyme. The change in methylene orientation calculated here is larger than was deduced previously (Sahlin et al., 1982; Gräslund et al., 1985), because uncertainty in the earlier work as to the magnitude of the smaller methylene hyperfine coupling constants of the *E. coli* enzyme did not allow accurate determination of the methylene conformation or of the C1 spin density.

Table II: Spin Densities and Methylene Angles

	E. coli RDPR	mouse RDPR	PSII $Y_D^\bullet$	Tyr- model
C_1	0.49	0.33	0.14–0.34	0.20–0.44
C_3, C_5	0.26	0.25	0.29	0.26
O	0.16	0.34	0.45–0.25	0.45–0.21
Θ_{H1} (deg)	32	0	4–51	4–47

(*2*) *Photosystem II.* $Y_D^\bullet$, the stable radical of PSII, has been studied extensively over the past 20 years. Its ESR spectrum has been measured in a number of experiments where different line shapes are expected and observed. Figure 3 shows six ESR spectra of $Y_D^\bullet$ under various conditions, together with simulations derived from a single set of hyperfine coupling constants (given in Table I) and the experimentally determined **g** tensor (Brok et al., 1985). The agreement between the experimental spectra and the simulations is very good, so these parameters certainly approach closely the true values. The process whereby this parameter set was determined and experimental data in its support are presented below.

(*a*) *Powder ESR Spectra and Simulations.* In these spectra, the molecules in the sample are randomly ordered and molecular motion is slow, so that so-called powder spectra with only partially resolved structure are observed (traces A–C, F). The spectrum in trace A has a line shape reported often for both liquid and frozen PSII suspensions, and we take it to be the true powder spectrum of $Y_D^\bullet$ (cf. Barry & Babcock, 1988). Random orientation achieved by adsorption of spinach PSII membranes to spherical anion-exchange beads resulted in an essentially identical spectrum (not shown). Orientation of the photosystem II membranes can be achieved by drying a suspension on mylar film (Rutherford, 1985). For these oriented samples, the observed spectra depend on the angle between the magnetic field and the membrane (traces D and E). In liquid aqueous suspensions of membranes, particularly of stacked thylakoid membranes, an intermediate situation can obtain, where the molecules show some orientation (Berthold et al., 1981; Barry & Babcock, 1988), so these spectra are somewhat less suitable for detailed analysis. In cyanobacteria, however, PSII does not segregate into stacked membranes, and we expect orientation of cyanobacterial PSII to be less than spinach PSII and that the resulting spectra will reflect the true, unoriented powder spectrum. The spectra obtained from whole cells at room temperature (Barry &

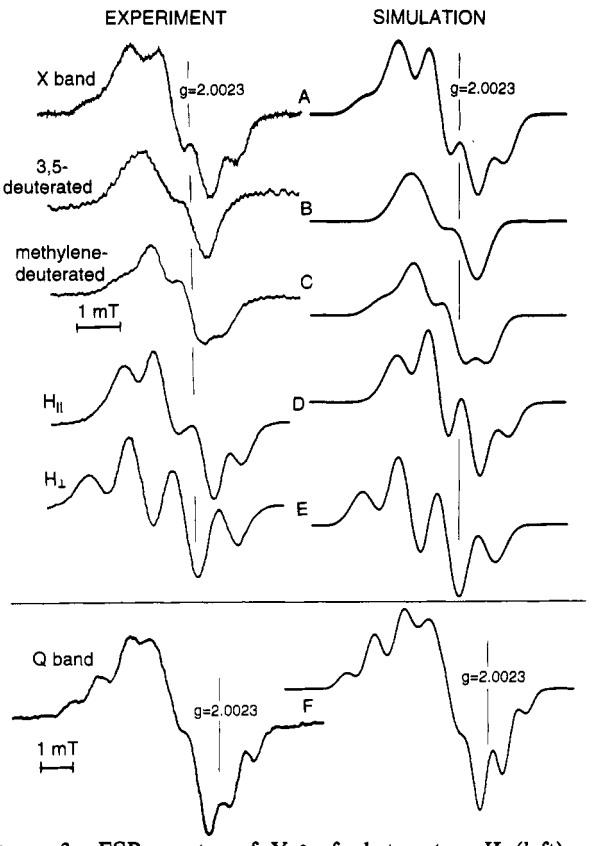

FIGURE 3: ESR spectra of $Y_D^\bullet$ of photosystem II (left) and corresponding simulations (right): (A) unlabeled unoriented, (B) 3,5-deuterated, (C) methylene-deuterated, (D) oriented with magnetic field parallel to the membranes, (E) oriented with magnetic field perpendicular to the membranes, all at X band; and (F) Q band. Traces B and C are from Barry et al. (1990), traces D and E are from Rutherford (1985), and trace F is from Brok et al. (1985) and has been plotted with a different horizontal scale than the X-band spectra. One millitesla = 10 G.

Babcock, 1988; Barry et al., 1990) are consistent with this expectation.

Cyanobacterial PSII samples containing specifically deuterated tyrosine were examined (Barry et al., 1990), and this deuteration, in general, collapses the hyperfine structure (traces B and C). As in the case for *E. coli* RDPR, the $Y_D^\bullet$ spectrum is dominated by hyperfine interaction with the 3,5 ring protons and with one methylene proton (Barry et al., 1990); deuteration at the 2,6 positions causes essentially no change in the line shape. Spectra obtained at higher microwave frequency (trace F), and therefore higher static magnetic field, show additional splitting due to the increased importance of anisotropy in the **g** tensor (Brok et al., 1985; Gulin et al., 1992).

The 3,5-deuterated spectrum shows only one partially resolved hyperfine splitting, which disappears on total deuteration of the tyrosine and is due to a methylene proton (Barry et al., 1990). One expects β-proton couplings to be nearly isotropic, and that is consistent with our simulations. On the basis of the line shape and overall peak-to-trough line width, we find a coupling of about 8 G for this proton. This value contrasts with our previous assignment for the methylene proton coupling of 10.5 G (Barry et al., 1990), which was based upon ENDOR spectroscopy (O'Malley et al., 1984). In the following section, we have investigated this coupling in detail, by using ENDOR spectroscopy and specifically deuterated samples.

Simulations of the methylene-deuterated spectrum and the fully protonated powder spectrum at X-band are useful for fixing the principal values and orientation of the 3,5 hyperfine

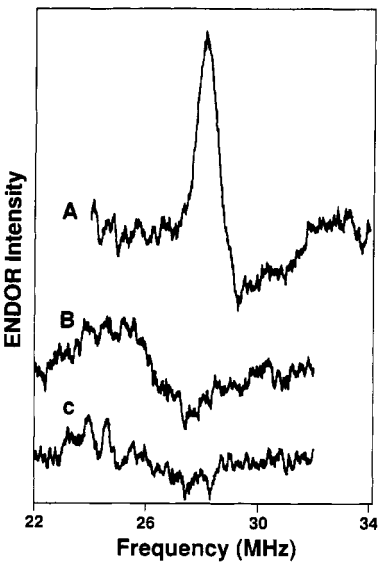

FIGURE 4: ENDOR of $Y_D^\bullet$ in isolated PSII. (A) Spinach; (B) protonated *Synechocystis*; (C) methylene-deuterated *Synechocystis*. Spectra were recorded at −140 °C.

tensors. In our simulations, we started by assuming that we could scale, by the same factor, the three principal values obtained by ENDOR for *E. coli* RDPR. We found that the calculated spectra are not very sensitive to small changes that maintain constant the sum of A_x and A_z (not shown). Further simulations indicate that the 3,5 hyperfine tensors are not collinear with the C–H bond, probably because of dipolar coupling with spin at the oxygen, as in eukaryotic RDPR. As in the case of RDPR, this effect shows up most clearly in the shoulder at low field.

The second methylene proton should have a nearly isotropic coupling that can be given an upper limit of 2.5 G; larger values noticeably distort the computed spectra (not shown). From this upper limit and eq 1, we can determine the range of possible values for the dihedral angles and the spin density on C1: $4° \leq \theta_{H1} \leq 51°$ and $0.14 \leq \rho_C \leq 0.34$. Even if the actual values lie at the upper end of these ranges, we conclude that $Y_D^\bullet$ has significantly lower spin density at C1, and correspondingly higher spin density at the oxygen, than has *E. coli* RDPR.

(*b*) *ENDOR Spectroscopy.* A methylene proton coupling (A_{iso} = 10.5 G) was deduced from a strong line between 28 and 30 MHz in the ENDOR spectrum of $Y_D^\bullet$ that had a line shape reminiscent of an axial tensor (O'Malley et al., 1984). In spinach PSII preparations, this line shape is reproducible (Figure 4, trace A). Our simulation results are inconsistent with this assignment, however, as indicated above. Rather, our analysis indicates that this ENDOR line derives from the 3,5 protons and that the 8-G coupling to the methylene proton should lead to an ENDOR signal at about 26 MHz.

Ring α protons, such as the 3,5 protons in $Y_D^\bullet$, are usually difficult to detect by ENDOR in unoriented solid samples, because of broadening from the relatively large hyperfine anisotropy inherent to this class of protons (Hyde et al., 1968; O'Malley & Babcock, 1986). In the case of spinach PSII, it appears that the hyperfine field felt by these protons is about as strong as the externally applied magnetic field. This equivalence of internal and external fields leads to the appearance of "forbidden" lines in ESR (Wertz & Bolton, 1986), as the nuclear spin eigenstates are not the same in the two electron spin manifolds (i.e., $m_s = +^1/_2$ and $m_s = -^1/_2$). The consequence for ENDOR is that an efficient cross-relaxation pathway is opened, and this relaxation pathway

defeats the usual kinetic bottleneck caused by slow nuclear-spin relaxation in the unpumped electron-spin manifold and leads to anomalously high ENDOR intensity. Such a situation has been observed and explained for the case of an α proton in a radical product in irradiated, single crystals of malonic acid (Brustolon & Cassol, 1984). For this radical, the ENDOR signal intensity is a strong function of the crystal orientation. The intensity maximum occurs at about twice the free proton Larmor frequency and falls off sharply as the effective hyperfine splitting to the α proton deviates from that value. This is the same spectral region where the strong ENDOR signal from $Y_D^\bullet$ occurs.

To test this hypothesis, we sought to observe ENDOR in specifically deuterated PSII. This approach requires the use of cyanobacteria (Barry & Babcock, 1987). Under conditions that gave both ESR and matrix ENDOR signals of comparable intensities to those observed in the preparation from spinach, fully protonated PSII isolated from *Synechocystis* did not show the strong ENDOR signal (Figure 4, trace B). Instead, weaker features were observed, including a derivative feature centered at 26 MHz, which is where the ENDOR signal from an 8-G coupling should appear. The absence of the strong ENDOR signal in the cyanobacterial preparation supports our hypothesis of anomalous ENDOR intensity. For the malonic acid radical, a small change in hyperfine splitting was sufficient to cause a large decrease in ENDOR intensity (Brustolon & Cassol, 1984). We suggest that the hyperfine tensors of the 3,5 protons in $Y_D^\bullet$ may be slightly different in spinach and *Synechocystis*.

To test whether the derivative-shaped feature at 26 MHz arises from the methylene proton, as suggested above, a methylene-deuterated *Synechocystis* PSII preparation was examined by ENDOR (Figure 4, trace C). As with the fully protonated sample, it does not show the strong line at 28–30 MHz. More importantly, the derivative-shaped feature at 26 MHz is lacking. This observation confirms our assignment of the methylene proton hyperfine coupling constant of 8 G. On the basis of the very weak, negative feature at 28 MHz, the 3,5 proton A_x component is about 9.5 G in *Synechocystis*, very similar to the value in RDPR. Reexamination of trace A in Figure 4 suggests that the A_x component of the 3,5 proton hyperfine tensor is about 11.3 G in spinach. Electron spin echo envelope modulation studies of spinach PSII show a low-frequency modulation that was attributed to a methylene proton with an isotropic coupling of 9.7 gauss (Evelo et al, 1989) but might, instead, be due to the 3,5 protons with one principal hyperfine component of 11.2 gauss.

(*c*) *Oriented Samples: Simulations and the Orientation of Y_D in the Membrane.* When BBY-type PSII membranes are dried onto mylar film, they orient with the membrane plane parallel to the plane of the film. The paramagnetic species of PSII are partially oriented in these samples, and their ESR spectra differ noticeably from the powder spectrum and reflect the partial orientation (O'Malley et al., 1984; Rutherford, 1985). These spectra can be used to test the hyperfine assignments made above. Furthermore, these spectra provide information that enables us to deduce the orientation of the tyrosyl ring plane in the membrane.

When the static magnetic field is aligned normal to the film and the membranes, it has a unique orientation in the molecular axis system of the radical and its corresponding **g** tensor. Therefore, for this orientation of the film, only one **g**-value contributes to the spectrum and a single-crystal-like spectrum results (Figure 3, trace E). This is evident in the experimental spectrum by the high degree of symmetry around the center of the spectrum. Perfect orientation of the sample is not achieved, so the spectrum has only four broad lines with a 1:3:3:1 intensity pattern. When the oriented membranes are rotated in the magnetic field, the spectrum becomes narrower and asymmetric and shifts to higher field. This shift in *g*-value indicates that the membrane normal lies nearer to the g_x axis than to either of the other two *g* axes. The change in line width indicates that the membrane normal lies near one of the A_x axes of the 3,5 hyperfine tensors.

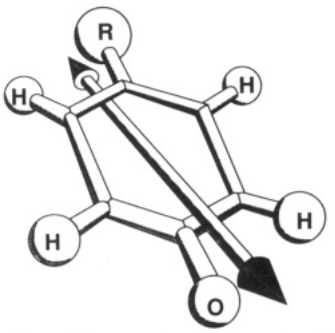

FIGURE 5: Orientation of the membrane normal with respect to the tyrosine phenoxyl ring of Y_D. Only one of four possible orientations is shown. See text for further details.

The line shapes of these two oriented spectra can be well simulated (Figure 3, traces D and E) when the membrane normal is assumed to have an orientation with respect to the **g** tensor (and, hence, the phenol headgroup) defined by the usual polar angles θ and Φ of 75° and ±10°, respectively, as shown in Figure 5. (θ is the angle between the membrane normal and the g_z axis, and Φ is the angle between the g_x axis and the projection of the membrane normal into the plane containing the g_x and g_y axes.) That the splitting patterns of both oriented spectra can be simulated with the same set of hyperfine tensors used in simulating the powder spectra is further evidence in its favor. Moreover, the θ and Φ values derived from the simulations indicate that the plane of the tyrosyl phenol ring is almost perpendicular to the plane of the membrane and, further, that the molecular axis containing C1, C4, and the phenolic O is about 20° away from the membrane normal. Exact reproduction of the reported *g*-values would necessitate an orientation a few degrees further from the g_x axis; this difference probably reflects small errors in the reported *g*-values and in the hyperfine parameter set used in the simulations. Whether the phenolic oxygen points toward the stromal or lumenal membrane surface cannot be determined from these spectra.

(*3*) *In Vitro Tyrosine.* Tyrosine radicals with specific deuterium substitution were formed by UV illumination of frozen solutions at high pH (Barry et al., 1990). These radicals gave spectra similar to but not identical to the corresponding spectra of $Y_D^\bullet$. These spectra can be simulated (not shown) by using the parameters given in Table I, which includes the **g** tensor determined experimentally (Fasanella & Gordy, 1969). The hyperfine coupling to one methylene proton is larger than found in PSII but smaller than in RDPR, and only an upper limit can be set for the smaller coupling. The 3,5 couplings are similar to those of *E. coli* RDPR, consistent with the absence of strong ENDOR intensity at twice the free proton Larmor frequency (M. El-Deeb, unpublished results). The calculated spin densities and dihedral angles can only be bracketed at present (Table II), but it is clear that the spin density at C1 is less than in *E. coli* RDPR.

DISCUSSION

Radicals in nonoriented proteins exhibit powder ESR spectra that are difficult to analyze because they consist of broad,

often poorly resolved features. It is usually not clear how many nuclei are involved, and, without other information, it is difficult to assign anisotropic (dipolar) interactions to the correct isotropic (contact) interaction. Isotopic labeling can be used to identify those nuclei that are coupled to the unpaired electron and ENDOR spectroscopy, because of its inherently higher resolution (Lubitz & Babcock, 1987), can provide detailed hyperfine information. A drawback to the latter technique, unfortunately, is its inherently low sensitivity. This is particularly acute for PSII samples, where only about 70 μM $Y_D^\bullet$ can be achieved, compared to radical concentrations of 0.5–1.5 mM that can be obtained in other amino acid radical-containing enzyme systems (e.g., Bender et al., 1989; Babcock et al., 1992). In the absence of clarifying information from isotope labeling and double-resonance techniques, however, simulations of EPR spectra are poorly constrained, and erroneous conclusions can be reached. For example, previous simulation analysis of the $Y_D^\bullet$ spectrum (Brok et al., 1985) was based on a plastoquinone cation radical origin for $Y_D^\bullet$ and led to a quite different set of hyperfine tensors: three of these tensors had large isotropic components, of which one also had a large dipolar contribution, while a fourth tensor had only a large dipolar contribution. It is interesting that neither the orientations of the dipolar components nor the magnitudes of the isotropic and anisotropic components are very different from those determined here. Although that parameter set was able to reproduce both the X-band and Q-band spectra and the two oriented spectra, it cannot simulate the isotopically substituted spectra (not shown). With the availability of the deuterium-substituted spectra (Barry et al., 1990), clear information identifying $Y_D^\bullet$ as a tyrosine radical (Barry & Babcock, 1987), and ENDOR data clarifying the methylene proton coupling (Figure 4), we have now been able to determine its larger hyperfine couplings (Table I).

From the analysis of the ESR spectra of $Y_D^\bullet$ and the other tyrosine radicals, we have obtained hyperfine information and, from that, information about the conformation and the spin density distribution of tyrosyl radicals in biologically significant environments (Table II). As has been obvious from our own and others' work, the conformation of the tyrosyl methylene group varies among proteins and is probably determined by steric factors within the protein. Thus, it is significant that $Y_Z^\bullet$ and $Y_D^\bullet$ have identical line shapes and that these two residues occur in the D1 and D2 polypeptides, respectively, in the middle of stretches of nine amino acids with nearly identical sequences (Debus et al., 1988). Current models of PSII (Trebst, 1985; Svensson et al., 1990) place these residues within membrane-spanning α-helical regions. Interactions with amino acid side chains three and four residues away in the sequence may, therefore, occur. Toward the membrane interior, these are phenylalanine and valine, while toward the membrane surface, these are glycine and glutamine.

Svensson et al. (1990) have developed a structural model for PSII by using computer modeling and sequence analogies with the bacterial photosynthetic reaction center. Their discussion of the surroundings of Y_D and Y_Z focuses on residues not within the same transmembrane segment. Their model suggests interactions with histidine 190 and with phenylalanine 186, which in cyanobacterial D2 is replaced by leucine. Sequence differences between cyanobacteria and spinach, therefore, may account for the slightly different hyperfine interactions that we have observed in the ENDOR spectra presented here. In their PSII structural model, the C1–C4–O direction of $Y_D^\bullet$ was proposed to lie 26° from the membrane normal, with the oxygen pointing out of the membrane toward the thylakoid lumen (Svensson et al., 1990). The membrane orientation we have determined for $Y_D^\bullet$ (Figure 5) is largely consistent with this model and provides an additional angular constraint on the geometry of the residue within the membrane, although there is no direct experimental evidence to determine whether the C1–C4–O axis points into or out of the membrane.

Previous analyses of the ESR spectra of $Y_D^\bullet$ indicated that partial orientation of the radical occurs in some aqueous suspensions (Berthold et al., 1981; Barry & Babcock, 1988). Our analysis suggests that a randomly oriented sample results from frozen suspensions (Figure 3, trace A). Deviations from the powder spectrum indicate partial orientation, so we conclude that static liquid suspensions of spinach thylakoid membranes (Berthold et al., 1981) experience partial orientation in the ESR spectrometer, whereas flowing thylakoid membranes or BBY membrane fragments show rather little orientation. Static thylakoid membranes tend to orient with the magnetic field perpendicular to the plane of the PSII-containing membranes. In that work, it was concluded that the membrane orientation of $Y_Z^\bullet$ was very nearly the same as that of $Y_D^\bullet$ (Berthold et al. 1981). Thus, Figure 5 provides a good representation of the $Y_Z^\bullet$ orientation also.

It is clear that the protein environment can alter the spin density distribution of the tyrosyl radical to a significant extent. Two factors that may be important in this are the electric charges around the radical and the presence or absence of a partner for hydrogen bonding. ENDOR has been used to address the hydrogen-bond status of RDPR, where none is present (Bender et al., 1989), and of $Y_D^\bullet$, where one is present (Rodriguez et al., 1987). This difference in local environment between the two radicals may contribute to the higher spin density at the phenol oxygen in $Y_D^\bullet$ compared to RDPR; the effects of hydrogen bonding on spin density distributions, however, are not yet well understood (e.g., Feher et al., 1985; Reiter et al., 1990).

The presence of electric charges near the radical site in RDPR can be determined because the B2 subunit containing the tyrosyl radical has been crystallized and structural information was published recently (Nordlund et al., 1990). The side chain of tyrosine 122, which bears the radical, is in van der Waals contact with side chains of four uncharged amino acids and one aspartic acid. This aspartic acid carboxyl group provides two coordinating oxygen atoms to one of the non-heme iron atoms in the subunit, and one of these oxygen atoms is the nearest atom to the tyrosyl oxygen, 0.33 nm away. We suggest that this negatively charged oxygen atom may also contribute to the low spin density at the phenoxyl oxygen and correspondingly high spin density at C1. The proximity of the tyrosine to the binuclear iron site is probably related to the function of the iron in producing the tyrosyl radical, which initiates the reaction with substrate. Although no crystal structure of PSII is available, computer modeling may again be consulted. Svensson et al. (1990) suggested that $Y_D^\bullet$ occupies a very hydrophobic environment of mainly phenylalanine and leucine side chains and one histidine that participates in the hydrogen bond to Y_D. The environment around Y_Z was suggested to be somewhat more hydrophilic. This may help explain the difference in their redox potentials and reactivity, but it apparently has little effect on spin densities, since the two PSII radicals have very similar spectra. We conclude that, among the radicals studied, *E. coli* RDPR is the one in which the spin density is most strongly perturbed by specific interaction with protein. From their studies of in vitro tyrosyl and other phenoxyl radicals, Sealy et al. (1985)

also concluded that the radical in *E. coli* RDPR has unusually strong methylene hyperfine coupling.

A complete description of the tyrosyl radicals in PSII will require more detailed ENDOR measurements, and we are pursuing these, as well as a more direct determination of the oxygen spin density, through the use of ^{17}O substitution. We also intend to pursue measurements of the Y_Z tyrosyl radical to elucidate the factors that govern the differences between it and Y_D in their thermodynamic and kinetic properties. Nevertheless, we can now state that the ESR line shape of the PSII tyrosyl radicals is understood.

ACKNOWLEDGMENT

We thank Matthew Espe, Matthew Gardner, Rita Bhatnagar, and Dr. Neil Bowlby for providing the photosystem II samples from *Synechocystis*. We acknowledge Dr. T. K. Chandrashekar for initiating the detailed characterization of $Y_D^{\bullet}$, Dr. Ivan D. Rodriguez for work with oriented PSII, and Drs. Mohamed El-Deeb and Peter Sandusky for helpful discussions.

REFERENCES

Babcock, G. T., Barry, B. A., Debus, R. J., Hoganson, C. W., Atamian, M., Sithole, I., & Yocum, C. F. (1989) *Biochemistry 28*, 9557–9565.

Babcock, G. T., El-Deeb, M. K., Sandusky, P. O., Whittaker, M. M., & Whittaker, J. W. (1992) *J. Am. Chem. Soc.* (in press).

Barry, B. A., & Babcock, G. T. (1987) *Proc. Natl. Acad. Sci. U.S.A. 84*, 7099–7103.

Barry, B. A., & Babcock, G. T. (1988) *Chem. Scr. 28A*, 117–122.

Barry, B. A., El-Deeb, M. K., Sandusky, P. O., & Babcock, G. T. (1990) *J. Biol. Chem. 265*, 20139–20143.

Bender, C. J., Sahlin, M., Babcock, G. T., Barry, B. A., Chandrashekar, T. K., Salowe, S. P., Stubbe, J., Lindström, B., Petersson, L., Ehrenberg, A., & Sjöberg, B.-M. (1989) *J. Am. Chem. Soc. 11*, 8076–8083.

Berthold, D. A., Babcock, G. T., & Yocum, C. F. (1981) *FEBS Lett. 134*, 231–234.

Brok, M., Ebskamp, F. C. R., & Hoff, A. J. (1985) *Biochim. Biophys. Acta 809*, 421–428.

Brok, M., Babcock, G. T., De Groot, A., & Hoff, A. J. (1986) *J. Magn. Reson. 70*, 368–378.

Brustolon, M., & Cassol, T. (1984) *J. Magn. Reson. 60*, 257–267.

Debus, R. J., Barry, B. A., Babcock, G. T., & McIntosh, L. (1988) *Proc. Natl. Acad. Sci. U.S.A. 85*, 427–430.

DeFelippis, M. R., Murthy, C. P., Faraggi, M., & Klapper, M. H. (1989) *Biochemistry 28*, 4847–4853.

DeFelippis, M. R., Murthy, C. P., Broitman, F., Weinraub, D., Faraggi, M., & Klapper, M. H. (1991) *J. Phys. Chem. 95*, 3416–3419.

Ehrenberg, A., & Reichard, P. (1972) *J. Biol. Chem. 247*, 3485–3488.

Evelo, R. G., Hoff, A. J., Dikanov, S. A., & Tyryshkin, A. M. (1989) *Chem. Phys. Lett. 161*, 479–484.

Fasanella, E. L., & Gordy, W. (1969) *Proc. Natl. Acad. Sci. U.S.A. 63*, 299–304.

Feher, G., Isaacson, R. A., Okamura, M. Y., & Lubitz, W. (1985) *Springer Ser. Chem. Phys. 42*, 174–189.

Fessenden, R. W., & Schuler, R. H. (1963) *J. Chem. Phys. 39*, 2147.

Ghanotakis, D. F., Demetriou, D. M., & Yocum, C. F. (1987) *Biochim. Biophys. Acta 891*, 15–21.

Gräslund, A., Sahlin, M., & Sjöberg, B.-M. (1985) *Environ. Health Perspect. 64*, 139–149.

Gulin, V. I., Dikanov, S. A., Tsvetkov, Yu. D., Evelo, R. G., & Hoff, A. J. (1992) *Proceedings of the ISE Conference*, Novosibirsk, 1991 (in press).

Harder, J., & Follmann, H. (1987) *FEBS Lett. 222*, 171–174.

Hyde, J. S., Rist, G. H., & Eriksson, L. E. G. (1968) *J. Phys. Chem. 72*, 4269–4276.

Janes, S. M., Mu, D., Wemmes, D., Smith, A. J., Kaus, S., Maltby, D., Burlingame, A. L., & Klinman, J. P. (1990) *Science 248*, 981–987.

Kurreck, H., Kirste, B., & Lubitz, W. (1988) *Electron Nuclear Double Resonance Spectroscopy of Radicals in Solution*, 1st ed., VCH Publishers, Inc., New York.

Leniart, D. S. (1979) in *Multiple Electron Resonance Spectroscopy* (Dorio, M. M., & Freed, J. H., Eds.) pp 5–72, Plenum Press, New York.

Li, Y. F., Heelis, P. F., & Sancar, A. (1991) *Biochemistry 30*, 6322–6329.

Lubitz, W., & Babcock, G. T. (1987) *Trends Biochem. Sci. 12*, 96–100.

Nordlund, P., Sjöberg, B.-M., & Eklund, H. (1990) *Nature 345*, 593–598.

Noren, G. H., Boerner, R. J., & Barry, B. A. (1991) *Biochemistry 30*, 3943–3950.

O'Malley, P. J., & Babcock, G. T. (1986) *J. Am. Chem. Soc. 108*, 3995–4001.

O'Malley, P. J., Babcock, G. T., & Prince, R. C. (1984) *Biochim. Biophys. Acta 766*, 283–288.

Prütz, W. A., Butler, J., Land, E. J., & Swallow, A. J. (1986) *Free Radical Res. Commun. 2*, 69–75.

Reiter, R. C., Stevenson, G. R., & Wang, Z. Y. (1990) *J. Phys. Chem. 94*, 5717–5720.

Rodriguez, I. D., Chandrashekar, T. K., & Babcock, G. T. (1987) in *Progress in Photosynthesis Research*, Proceedings of the 7th International Congress on Photosynthesis, 1986, (Biggins, J., Ed.) Vol. 1, pp 471–474, Nijhoff, Dordrecht, The Netherlands.

Rutherford, A. W. (1985) *Biochim. Biophys. Acta 807*, 189–201.

Rutherford, A. W., Zimmermann, J.-L., & Boussac, A. (1992) in *The Photosystems: Structure, Function, and Molecular Biology* (Barber, J., Ed.) pp 179–229, Elsevier Science Publishers, Amsterdam.

Sahlin, M., Gräslund, A., Ehrenberg, A., & Sjöberg, B.-M. (1982) *J. Biol. Chem. 257*, 366–369.

Sahlin, M., Petersson, L., Gräslund, A., Ehrenberg, A., Sjöberg, B.-M., & Thelander, L. (1987) *Biochemistry 26*, 5541–5548.

Scholes, C. P., Liu, Y., Fishel, L. A., Farnum, M. F., Mauro, J. M., & Kraut, J. (1989) *Isr. J. Chem. 29*, 85–92.

Sealy, R. C., Harman, L., West, P. R., & Mason, R. P. (1985) *J. Am. Chem. Soc. 107*, 3401–3406.

Sevilla, M. D., Yan, N., Becker, D., & Gillich, S. (1989) *Free Radical Res. Commun. 6*, 99–102.

Sivaraja, M., Goodin, D. B., Smith, M., & Hoffman, B. M. (1989) *Science 245*, 738–740.

Sjöberg, B.-M., & Gräslund, A. (1983) *Adv. Inorg. Biochem. 5*, 87–110.

Smith, W. L., Eling, T. E., Kulmacz,, R. J., Marnett, L. J., & Tsai, A. L. (1992) *Biochemistry 31*, 3–7.

Stubbe, J. (1989) *Annu. Rev. Biochem. 58*, 257–285.

Svensson, B., Vass, I., Cedergren, E., & Styring, S. (1990) *EMBO J. 9*, 2051–2059.

Trebst, A. (1985) *Z. Naturforsch. 41c*, 240–245.

Wertz, J. E., & Bolton, J. R. (1986) *Electron Spin Resonance Elementary Theory and Practical Applications*, Chapman and Hall, New York.

Wagner, A. F. V., Frey, M., Neugebauer, F. A., Schäfer, W., & Knappe, J. (1992) *Proc. Natl. Acad. Sci. U.S.A. 89*, 996–1000.

Whittaker, M. M., & Whittaker, J. W. (1990) *J. Biol. Chem. 265*, 9610–9613.